25 May 2000

ELSEVIER

Optics Communications 179 (2000) 137–148

OPTICS COMMUNICATIONS

www.elsevier.com/locate/optcom

Ballistic peaks at quantum resonance

W.H. Oskay, D.A. Steck, V. Milner, B.G. Klappauf [1], M.G. Raizen [*]

Department of Physics, The University of Texas at Austin, Austin, TX 78712-1081, USA

Received 27 August 1999; received in revised form 29 November 1999; accepted 21 December 1999

Abstract

We report studies of the motion of cold atoms in a time-dependent optical potential. The dynamics of our system are that of the quantum kicked rotor, and exhibit a wide variety of phenomena. One purely quantum effect is the quantum resonance, which occurs for well-chosen initial conditions and specific values of the period between kicks. Distinctly nonclassical behavior, such as ballistic growth in momentum, is possible at a quantum resonance. Previous experimental studies have observed these resonances, but have not clearly resolved the expected ballistic motion. We now observe ballistic motion at quantum resonances and compare our momentum distributions with theory and numerical simulations. © 2000 Elsevier Science B.V. All rights reserved.

PACS: 05.45.+b; 32.80.Pj; 42.50.Vk; 72.15.Rn
Keywords: Quantum chaos; Atom optics; Dynamical localization; Kicked rotor; Quantum resonance

1. Introduction

Quantum systems with nonintegrable classical limits have proven to be a rich field of study over the last quarter century. A natural focus of study has been the interface between the starkly different behavior in the classical and quantum regimes. This field of research, 'quantum chaos', has led to the discovery of fundamentally new quantum mechanical phenomena, which have in turn been areas of active research. One such result is dynamical localization, a quantum suppression of classical (chaotic) diffusion [1–7]. Another purely quantum effect is the quantum resonance, where a ballistic (quadratic), rather than diffusive, growth of energy can take place [8].

Dynamical localization was first studied experimentally in the ionization of Rydberg atoms in strong microwave fields [9–13]. A more recent experimental technique involves momentum transfer to cold atoms in time-dependent optical potentials [14]. This technique was used in a series of experiments in our group on dynamical localization and quantum chaos with cold sodium atoms [15–19]. These results, along with other work [20], established atom optics as a new experimental testing ground for the field. The simplest experimental configuration in that work was a periodically pulsed standing wave of light. This system constitutes an experimental realization of the

* Corresponding author.
E-mail address: raizen@physics.utexas.edu (M.G. Raizen).
[1] Present address: Institut Non Linéaire de Nice, 1361 route des Lucioles, 06560 Valbonne France.

0030-4018/00/$ - see front matter
PII: S0030-4018(00)00453-3

kicked rotor, which has widely been studied in classical and quantum chaos for many years.

A quantum resonance is a phenomenon that occurs in the kicked rotor system when the time between kicks is carefully chosen. Then, for certain initial conditions, the evolution operator between kicks can become either unity or only alternate sign between successive kicks. Quantum resonances were observed in experiments with sodium atoms using this idea [15,21]. In contrast to the ballistic motion expected when the evolution operator becomes unity, it was observed that near the quantum resonances most of the momentum distribution rapidly settled into a nearly static distribution. This is primarily due to the nonzero initial momentum width of the distribution. A small fraction of the atoms appeared to undergo ballistic motion, but the signal was below the available resolution of the experiments [21].

Our current set of experiments are conducted with a second generation system that uses cesium atoms [22]. This experiment has considerably higher resolution than those using sodium atoms, and we are now able to clearly resolve ballistic peaks at the quantum resonance. Our study is relevant not only for comparison with theory, but also in relation to ongoing studies about effects of applied acceleration in this system. Quantum resonances have been studied in this context [23], where it was found that gravity in the direction of the standing wave can enhance ballistic motion.

In the remainder of this paper we will first introduce a theoretical description of our system. We will then describe the experimental setup before presenting our results.

2. Theoretical background

Our experiments are performed on cold atoms that interact with a pulsed standing wave of light. We begin by showing the connection between this system and the kicked rotor problem.

Let us consider a two-level atom with transition frequency ω_0 interacting with a standing wave of linearly polarized, monochromatic light of frequency ω_L, and let $k_L = \omega_L/c$. This light forms a one-dimensional optical lattice of the type that is now commonly used in atom optics. We are concerned with the limit where the laser detuning $\Delta_L = \omega_L - \omega_0$ is large relative to the relaxation rate Γ of the excited state. In this case, the induced dipole force due to the AC Stark shift can be significant while incoherent effects such as spontaneous emission can be made negligible. Furthermore, the excited state population can be adiabatically eliminated [14]. In this approximation, we neglect internal structure and treat the atom as a point particle. This approximation leads to the following Hamiltonian for the center-of-mass motion of the atom:

$$H(x,p) = \frac{p^2}{2m} + V_0 \cos(2k_L x). \tag{1}$$

Here, m is the atomic mass, $V_0 = \hbar\Omega^2/8\Delta_L$ is the 'well depth' of the lattice, $\Omega = -2d_z E_0/\hbar$ is the maximum Rabi frequency, $\boldsymbol{d}$ is the atomic dipole moment, and E_0 is the electric field of a single traveling wave component of the standing wave $\boldsymbol{E}(x,t) = \hat{z}2E_0\cos(2k_L x)\cos(\omega_L t)$.

The behavior described so far corresponds to the dynamics of the simple pendulum. We may introduce time dependence by changing the well depth, which is easily controlled by changing the intensity of the standing-wave light. The kicked rotor corresponds to the case where the optical field is pulsed on periodically in time:

$$H(x,p,t) = \frac{p^2}{2m} + V_0 \cos(2k_L x) \sum_n F(t-nT). \tag{2}$$

Here, T is the kicking period, and $F(t)$ is a pulse shape function of unit amplitude and duration $t_p \ll T$. In the limit of δ-function pulses, we recover the Hamiltonian of the δ-kicked rotor. In a physical experiment one cannot reach this limit, and the nonzero pulse lengths lead to a decreasing effective kick amplitude as a function of atomic momentum [22].

It is convenient to transform to a set of scaled, dimensionless units. Let us define $x' = 2k_L x$, $p' = (\bar{k}/2\hbar k_L)p$, $t' = t/T$, $f(t') = F(Tt')/\eta$, $K = (\bar{k}/\hbar)\eta V_0 T$, and $H' = (\bar{k}/\hbar)TH$, so that we may rewrite the kicked rotor Hamiltonian (2) as

$$H(x,p,t) = \frac{p^2}{2} + K\cos(x) \sum_n f(t-n), \tag{3}$$

after dropping the primes. In these transformations, we have defined the pulse integral $\eta = \frac{1}{T}\int_{-\infty}^{\infty} F(t)\mathrm{d}t \propto t_p/T$ and the constant $\bar{k} = 8\omega_r T$, where $\omega_r = \hbar k_L^2/2m$ is the recoil frequency. We will use these scaled variables for the remainder of this paper, except for the presentation of data in which momentum is reported in multiples of two photon recoils ($2\hbar k_L$). This momentum scale is natural since the dipole force arises from the scattering of photons from one traveling wave into the other and the atomic momentum can only change by two photon recoils (by $\bar{k}$ in scaled units) at a time. This 'momentum ladder' structure also results from the spatial periodicity of the potential.

The classical dynamics of the ideal δ-kicked rotor are given by the Chirikov–Taylor map, or 'standard map', obtained by integrating over a single kicking period. The dynamics are completely specified by the stochasticity parameter K. For $K > 4$, the phase space is predominantly chaotic. The signatures of chaotic behavior in an ensemble of rotors are approximately diffusive (linear) energy growth in time and a Gaussian momentum distribution.

The quantum dynamics are specified by K as well as by the additional parameter $\bar{k}$. The scaled commutation relation is $[x, p] = i\bar{k}$, and we interpret $\bar{k}$ as a scaled Planck constant that measures the action scale of our system relative to $\hbar$. The system exhibits diffusive behavior only for short times, after which the rotors settle into an exponential momentum distribution [2,5], the hallmark of dynamical localization.

Quantum resonances have been studied theoretically, and it was found that if the period T between pulses is carefully chosen, the system is not expected to exhibit dynamical localization. Between kicks, the atoms undergo free evolution for a fixed period. During this evolution, a plane wave with momentum p_0 accumulates a quantum phase proportional to its energy and evolves by a phase factor $\exp[-ip_0^2/2\bar{k}]$. During a kick, the atom is only free to couple to other plane waves on its momentum ladder, i.e., those with momentum $p_0 \pm j\bar{k}$, where j is an integer. When the initial momentum p_0 is either zero or an integer multiple of $\bar{k}$, then a proper choice of $\bar{k} = 8\omega_r T$ can lead to phase factors of ± 1 for the free evolution for all states on the momentum ladder. This condition is called a quantum resonance and occurs when $\bar{k}$ is chosen to be an integer multiple of 2π [8]. Similar types of quantum resonant behavior are expected to occur at other rational multiples of $\bar{k}/2\pi$, although we have experimentally resolved only the stronger resonances at integer values of $\bar{k}/2\pi$. For values of $\bar{k}$ that are even multiples of 2π, the free evolution factor is unity. For odd multiples of 2π, the phase factor either is unity or flips sign between successive kicks, depending on the initial momentum state.

At the quantum resonance where the evolution factor is unity for the $p = j\bar{k}$ plane waves (e.g., $\bar{k} = 4\pi$), the atoms should exhibit ballistic motion in which the energy grows quadratically with time [8,24,25]. We may illustrate this behavior by first considering the interaction between the atoms and a single pulse of light. Let us continue to use the case of a plane wave ($p_0 = 0$) initial condition and further simplify to the limit of a δ-function pulse. The probability for the atom to be diffracted into the momentum state with momentum $p = j\bar{k}$ is

$$P_j = J_j^2\left(K/\bar{k}\right), \tag{4}$$

where $J_n(x)$ is an ordinary Bessel function and j is an integer [26]. Let us now consider a series of N pulses timed so as to satisfy the quantum resonance condition. Since this condition 'collapses' the free evolution between the kicks, we can consider the pulse sequence to be a single large pulse. The momentum distribution after N kicks is thus

$$P_j = J_j^2\left(NK/\bar{k}\right). \tag{5}$$

The evolution of this distribution is plotted in Fig. 1 for typical experimental parameters. The Bessel functions $J_n(x)$ peak when x is near n, and two clear peaks move out from $p_0 = 0$ at a uniform rate. It is important to note that while these peaks do represent the leading edge of the probability distribution, they do not represent uniform acceleration of the entire atomic sample. Two features of Fig. 1 that illustrate this are the low absolute amplitudes of the peaks and the rich structure between the peaks, as is clear on the density plot.

This analysis has considered only a plane-wave initial condition at $p_0 = 0$, so that the momenta are restricted to the integer momentum states $p = j\bar{k}$ (for

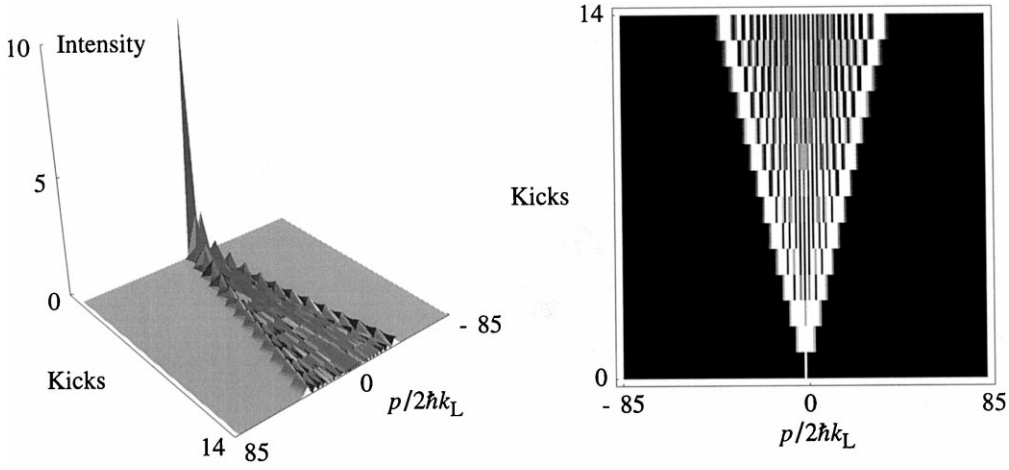

Fig. 1. Ballistic peaks in the δ-kicked rotor with a plane-wave initial condition and parameters $\bar{k} = 4\pi$ and $K = 37$. Two peaks move away from $p_0 = 0$ with near uniform acceleration. The distributions shown are calculated from Eq. (5). The evolution of the momentum distribution is shown as both a surface plot (left) and as a density plot (right). The intensity scale for these plots is linear.

integer j). This assumption is valid in the case of the kicked *rotor*, where most of the relevant theoretical work has been done. However, given the continuous nature of our experiment, this model is of limited utility, as we will show.

Fig. 2 compares the effects of using plane-wave and Gaussian initial conditions in numerical simulations at $\bar{k} = 2\pi$. In this case we expect to see quantum 'antiresonance' behavior where the flipping of sign between successive kicks causes periodic recurrences. While this behavior is observed for a plane wave initial condition, the continuous distribution shows surprisingly different results. In the Gaussian case, we see a nearly static central region flanked by two weak ballistic peaks. It is clear from these results that the choice of initial conditions can make a large difference in the observed dynamics. Indeed, the primary signature of quantum resonances in the earlier sodium experiments was a static, rather than accelerating, momentum distribution [15,21]. In those experiments, no difference was observed between the behavior of the system at $\bar{k} = 2\pi$ and 4π.

A more detailed consideration of the dynamics can be used to account for both momentum ladders with $p_0 \neq 0$ as well as the initial momentum distribution of the atomic sample [21]. Independent of these considerations, atoms initially near $p = 0$ will undergo ballistic motion as we have described, for $\bar{k} = 4\pi$. The overall behavior leads to momentum distributions characterized by a static central region surrounded by ballistic peaks, as our results in this study indicate.

One other fundamental difference between our system and the ideal δ-kicked system is the nonzero pulse length in our experiment [22]. If we continue to view the pulse sequence as a single large pulse, then we note that the movement of atoms during the total pulse time may no longer be negligible. The motion of atoms in a nonlinear resonance is bounded, and we expect this boundary to play some role in our observed distributions [18]. A second complication is that our pulse period T (defined from the beginning of one kick to the beginning of the next one) is not exactly equal to the time *between* kicks. A consequence of these effects is that there is some subtlety in comparing our experiments with theory based on δ-kicks. The finite-pulse effects are accounted for by directly incorporating them into numerical quantum simulations that use experimental parameters such as the pulse length. We employ these simulations for unambiguous comparison between theory and experiment in the remainder of this paper.

The numerical simulations in the vicinity of the quantum resonance proved to be particularly sensi-

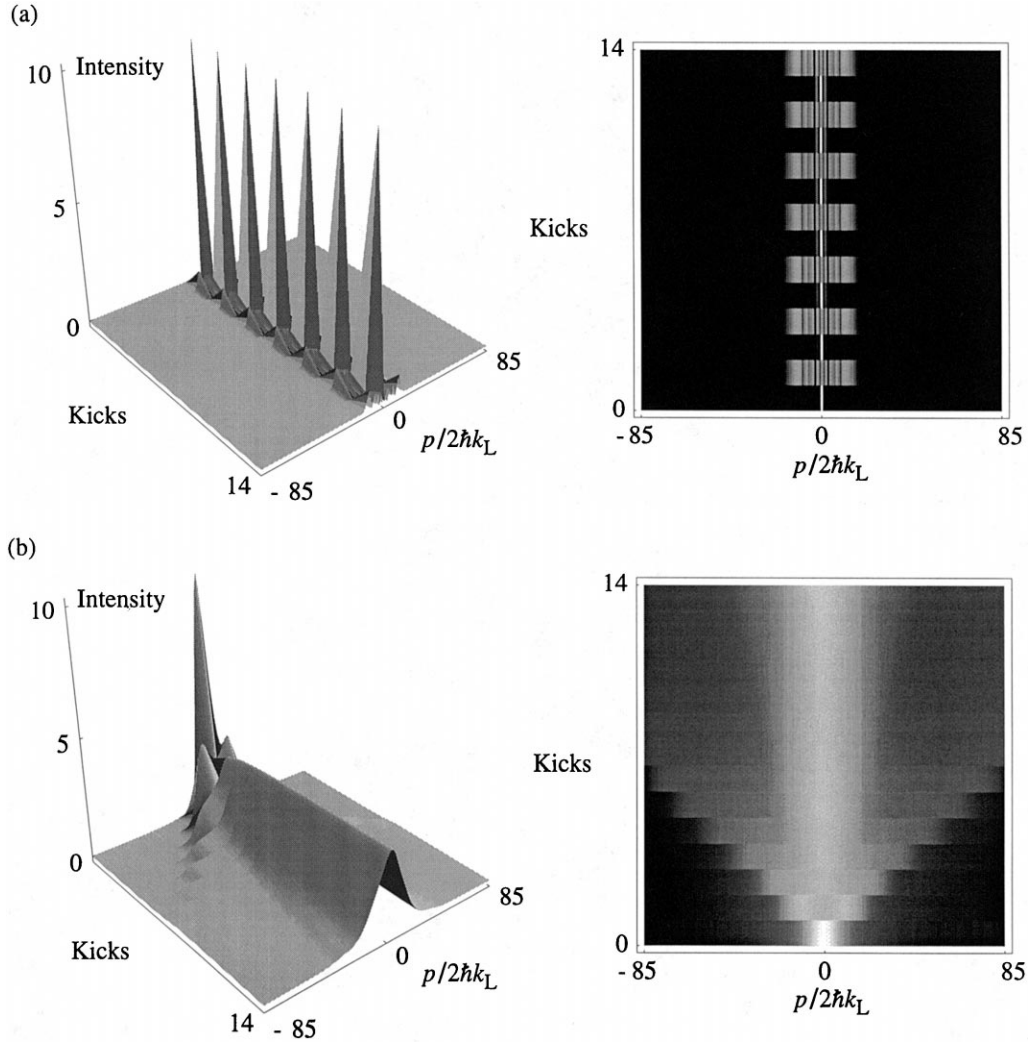

Fig. 2. Comparison of quantum δ-kicked rotor simulations at $\bar{k} = 2\pi$ and $K = 82$. Part (a) shows a simulation with a plane wave ($p_0 = 0$) initial condition. This case shows quantum 'antiresonance' behavior characterized by period-2 recurrences and a lack of ballistic peaks. Part (b) shows a simulation for the same parameters, but beginning with a near-Gaussian initial momentum distribution of width $\sigma_p/2\hbar k_L = 4$. This distribution was obtained from a time-of-flight measurement and is very close to that used in the experiments. In this case, ballistic peaks are visible and the overall dynamics are more complicated. The intensity scale for the surface plots (left) is linear while the intensity scale for the density plots (right) is logarithmic.

tive to the chosen ensemble and grid resolution. We will describe these simulations in some detail because high resolution is required to eliminate numerical artifacts and ensure that the calculated distributions converge. The simulations in this paper with near-Gaussian initial conditions (Fig. 2b and Fig. 6) were started with a distribution that is very close to the initial condition in our experiment. An ensemble of 30 wavepackets (50 for Fig. 6(d–f)) was distributed uniformly along a unit cell in position. The momentum distribution for each packet was directly adapted from a recent time-of-flight momentum measurement of the initial condition in our experiment. These simulations were performed on a grid

spanning the range $p/2\hbar k_L = \pm 256$. The grid resolution was $\Delta p/2\hbar k_L = 1/1024$ and the plots were smoothed by averaging over bins of $2\hbar k_L$. For Fig. 6, the pulses were modelled by square pulses, and we have found that the simulations are not highly sensitive to the exact pulse shape.

3. Experiment

The experimental setup is that of our earlier studies of quantum chaos with cesium atoms [22,27,28], with modifications primarily to the parameters under study. The experiments are performed on laser-cooled cesium atoms in a magneto-optic trap (MOT) [29,30].

Two actively locked, single-mode diode lasers at 852 nm are used for cooling, trapping, and detection of the cesium atoms. The trapping light is produced by the first laser and is tuned 15 MHz to the red of the $(6S_{1/2}, F = 4) \rightarrow (6P_{3/2}, F' = 5)$ cycling transition. The light produced by the second laser is tuned to the center of the $(6S_{1/2}, F = 3) \rightarrow (6P_{3/2}, F' = 4)$ resonance. This repumping light is used to prevent optical pumping into the $F = 3$ ground state during the trapping and detection stages of the experiment. The trap is loaded at these parameters for 7 s. The atoms are further cooled by reducing the intensity of the trapping light and increasing its detuning for 3 ms before turning off the trapping light. We ensure that nearly all the atoms are in the $(6S_{1/2}, F = 4)$ ground state before the interaction with the standing wave by turning off the repumping light 150 μs after the trapping laser light. Typically, this procedure yields 10^6 atoms with $\sigma_x = 0.15$ mm. The momentum distribution is nearly thermal, and 96% of the distribution fits into a Gaussian of width $\sigma_p/2\hbar k_L = 4$, corresponding to a temperature of roughly 10 μK.

After the trapping fields are turned off, the interaction potential is turned on. The pulsed standing wave is provided by a stabilized, single-mode Ti:sapphire laser, which is pumped by an argon-ion laser. This light passes through an acousto-optic modulator that controls the pulse sequence. The beam is horizontally aligned with the atoms and retro-reflected through the chamber to form a standing wave. The beam has a typical maximum power of 470 mW at the chamber and a waist of 1.46 mm. We detuned this beam 6.1 GHz to the red of the $(6S_{1/2}, F = 4) \rightarrow (6P_{3/2}, F' = 5)$ cycling transition, with typical drifts of about 100 MHz. The pulse sequence consists of a series of 295 ns (full width at half maximum) pulses with a rise and fall times of about 70 ns. There is typically less than 3 ns variation in the pulse duration. The pulse period for the experiments presented here were chosen between $T = 20$ and 121 μs, corresponding to the range $\bar{k} \sim 2$ to 4π, with less than 4 ns variation per pulse period. The detection of momentum is accomplished by letting the atoms drift in the dark for a controlled duration (typically 15 ms). The trapping beams are then turned on in zero magnetic field, forming an optical molasses that freezes the position of the atoms [15]. The atomic position is recorded via fluorescence imaging in a short (10 ms) exposure with a cooled CCD camera. The final spatial distribution and the free-drift time enable the determination of the momentum distribution in the direction of the standing wave.

There are several systematic effects in the determination of the momentum distributions, which we now summarize. The first is the uncertainty in the spatial calibration of the imaging system. The second effect arises from the ambiguity in the drift time due to motion occurring during different interaction times. There is no clear way to remove this effect from the measured distributions. These two factors lead to overall systematic errors on the order of $\pm 10\%$ in the momentum scaling. Another effect that we must consider is due to the Gaussian intensity profile of the optical molasses laser beams used in the detection of the distributions. This leads to a slight reduction in the measured population in the wings of the momentum distributions. The energy $\langle p^2 \rangle$ of a momentum distribution tends to be particularly sensitive to the population at high momenta. It is primarily important to correct for these effects when energy of the distributions is to be calculated. However, for the purposes of this paper we are only concerned with the qualitative behavior of the distributions and the data presented here have not been compensated for these effects. A final systematic effect in our experiment concerns the strength of the interaction potential. The uncertainty in the stochasticity parameter K is $\pm 10\%$, with the largest contributions due to the measurement of laser beam profile and absolute power.

4. Data and results

Let us first examine the dynamics of our system in the absence of quantum resonances. Fig. 3 shows the evolution of a distribution when the kicking period was set to $T = 20$ μs, corresponding to $\bar{k} = 2.08$, which is not close to an integer multiple of 2π. In this case, the momentum distribution takes only a few kicks to settle into a distribution that is exponential over more than two orders of magnitude. This behavior is a signature of dynamical localization, which takes place when the quantum resonance condition is not satisfied. Note that values of the stochasticity parameter K reported here are not scaled according to the quantum scaling factor [28], which goes to zero in the vicinity of a quantum resonance.

As we tune to the quantum resonances, qualitatively different momentum distributions are found. Fig. 4 shows the behavior of the system near quantum resonances. The behavior near the antiresonance is shown in Fig. 4a. This data set was taken with pulses spaced by $T = 60$ μs, corresponding to $\bar{k} = 6.24 \sim 2\pi$, with stochasticity parameter $K = 19$. The distribution is nearly static. Note, for example, that the amplitude of the distribution is almost constant after the first kick. The overall shape of the distribution appears to remain that of the initial distribution. A slight ripple on the sides of the distribution can be identified as a ballistic peak. Fig. 4b shows the results of an experiment using pulses spaced by $T = 121$ μs, corresponding to $\bar{k} = 4\pi$, and with stochasticity parameter $K = 37$. The qualitative behavior is similar to the antiresonance ($\bar{k} = 2\pi$) case. The higher kicking strength appears to increase the population that undergoes ballistic motion, as one may infer from the larger bump on the right side of Fig. 4b. From a simplistic viewpoint, one might expect to see contrasting behavior in the cases of the resonance and antiresonance. However, as we saw in Fig. 2, the continuous nature of the initial condition has a strong effect on the evolution of the distributions. Some qualitative differences between the two cases do become visible in a regime of higher kicking strength, as we will see later. The parameters of this data set match those used to produce Fig. 1. It is apparent that the speed at which the ballistic peaks move out in both parts of Fig. 4 is approximately the same as in Fig. 1, where the peaks are at about $p/2\hbar k_L = \pm 40$ after 13 kicks. This is to be expected since the ratio $K/\bar{k}$ was approximately the

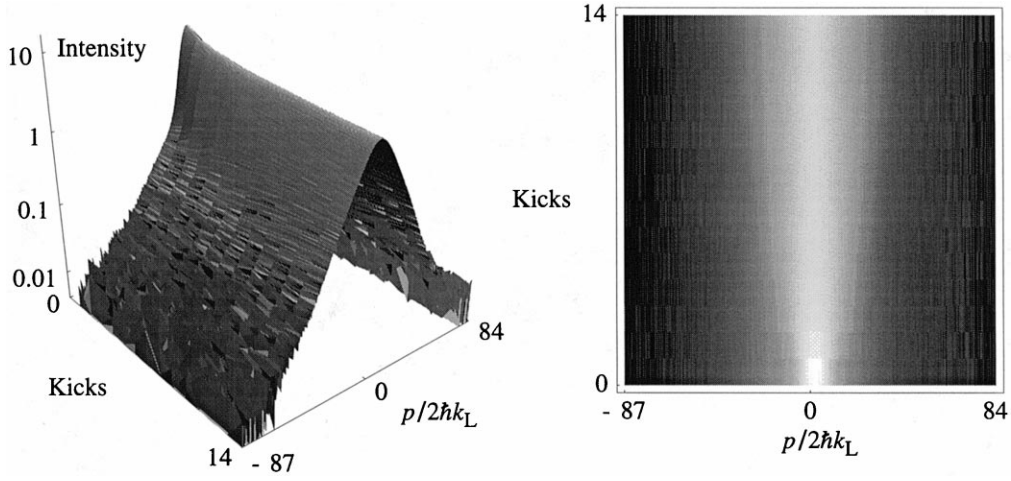

Fig. 3. Measured evolution of the momentum distribution as a function of time from the initial condition (0 kicks) through 13 kicks. For this scan, the parameters were $K \sim 10$ and $T = 20$ μs, corresponding to $\bar{k} = 2.08$. This corresponds to a parameter regime far from quantum resonances where dynamical localization is observed. The final profile shows a clear exponentially localized momentum distribution. Note that the intensity axis is logarithmic and in arbitrary units, and that each waveform has been normalized. The momentum axis is determined experimentally and the minor asymmetry is due to the initial position of the trapped atoms.

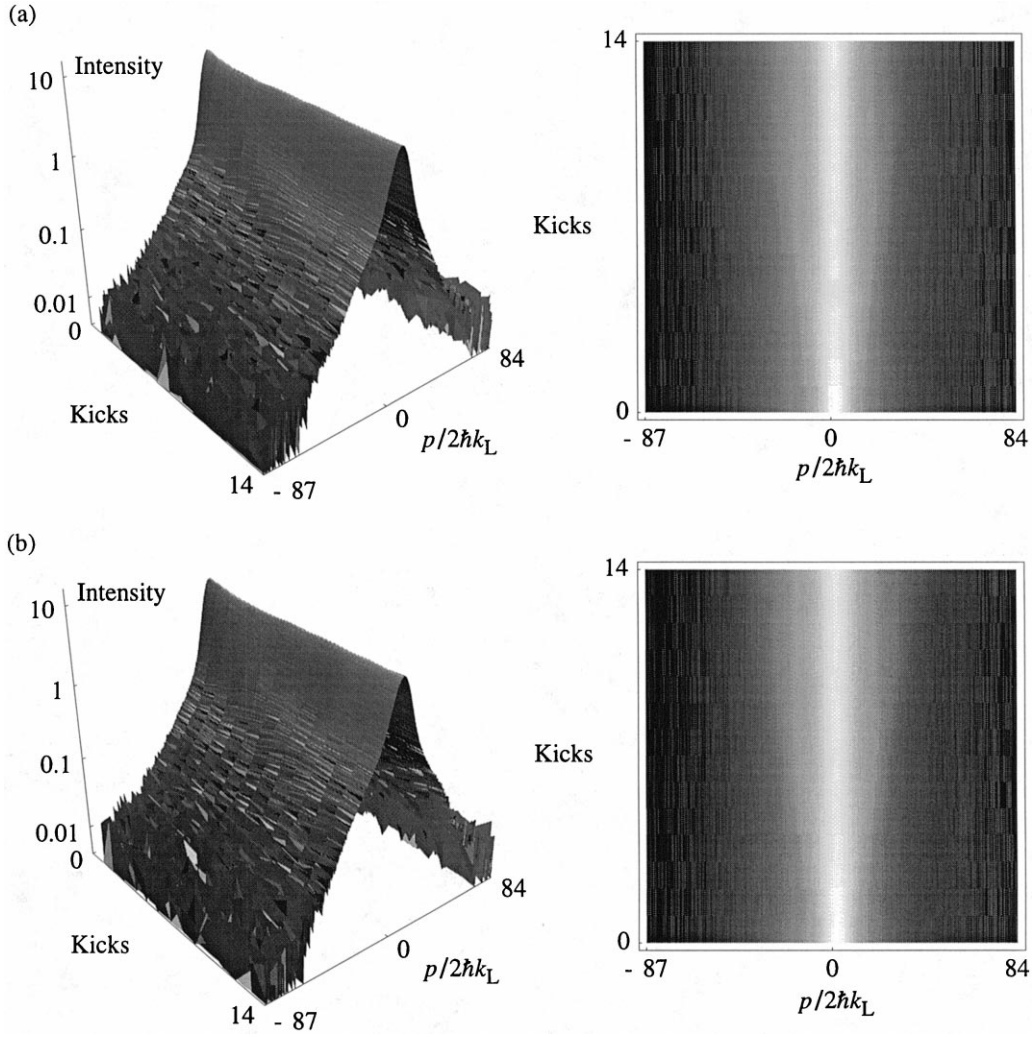

Fig. 4. Evolution of momentum distributions (a) near $\bar{k} = 2\pi$, with $K = 19$ and (b) near $\bar{k} = 4\pi$, with $K = 37$. The distributions are qualitatively different from the exponentially localized case shown in Fig. 3, and exhibit weak ballistic peaks. The peaks can be seen in this case as small ripples on the surface plots (left) that start at $p = 0$ and are visible as bulges at $p \approx \pm 40$ after 13 kicks. A second feature to notice is that the spread in p of the entire distribution is much smaller than in the localized case. The intensity scales for these plots are logarithmic and in arbitrary units.

same in the three cases. Note that the laser intensities for the data in Fig. 4a and Fig. 4b were approximately the same.

If we now turn up the stochasticity parameter, we can further increase the population that undergoes ballistic motion. Fig. 5 shows two cases with stronger kicks and more obvious ballistic peaks. Fig. 5(a–c) again shows the antiresonance case, with $T = 60.5$ μs. There are several features to note in this plot. First, the ballistic peaks are much larger than those in Fig. 4 and can now be clearly resolved. The peaks are also moving more quickly than those shown in Fig. 4. Here, the majority of the ballistic atoms have left the region in which we can detect atoms ($\approx \pm 80 \cdot 2\hbar k_L$) by the 10th kick. Since the distributions are normalized after detection, the remaining distribution appears to be inflated. For this data set only (Fig. 5(a–c)), a longer pulse width t_p of ap-

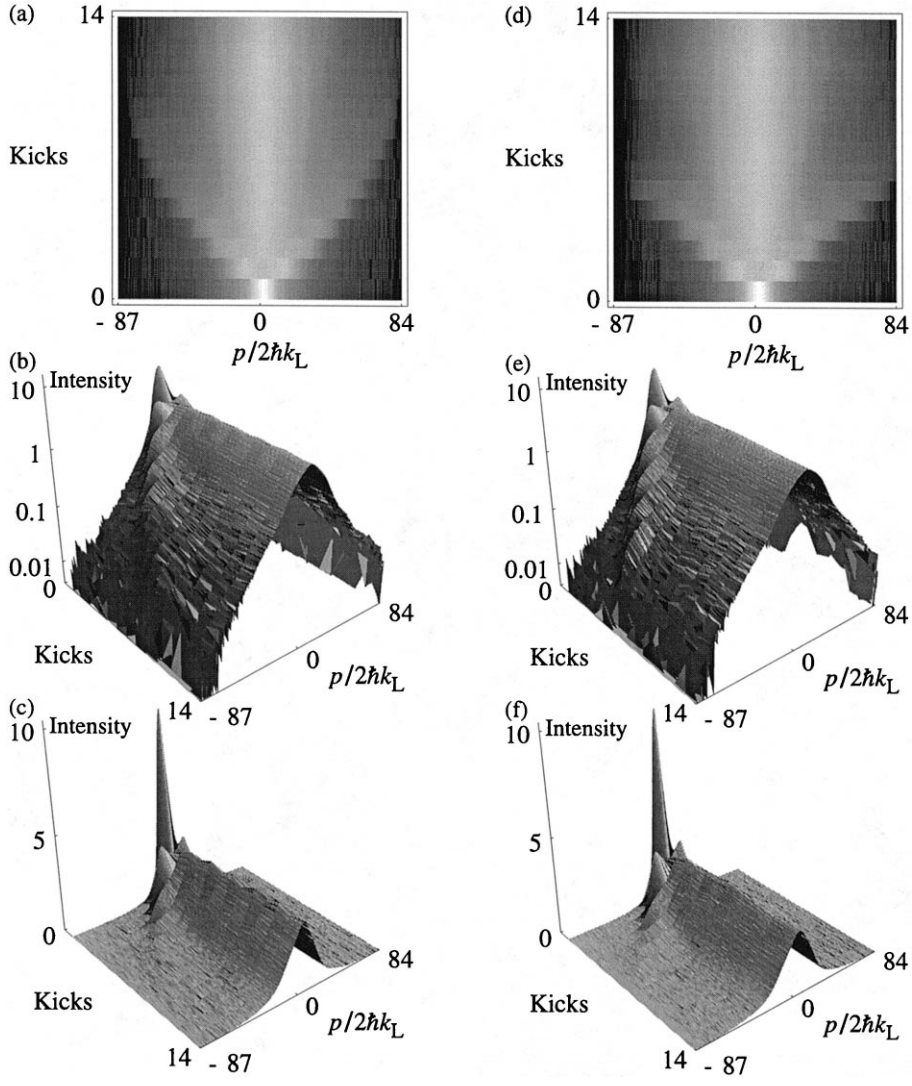

Fig. 5. Evolution of momentum distributions (a–c) near $\bar{k} = 2\pi$, with $K = 82$ and (d–f) near $\bar{k} = 4\pi$, with $K = 184$. The ballistic peaks are clearly visible in these plots. Finite pulse effects lead to a curvature in the apparent trajectory of the peaks for the $\bar{k} = 2\pi$ case. While the density plots (a,d) are shown with a logarithmic intensity scale, the surface plots are shown with both logarithmic (b,e) and linear (c,f) intensity scales to highlight different features. Each plot is in arbitrary units.

proximately 600 ns was used to further increase K. The longer pulse also leads to more pronounced finite-pulse effects, which are clearly visible in this plot. The peaks follow a path that is consistent with ballistic motion for the first few kicks, but slow down by about the seventh kick. The overall shape of the final distribution is similar to that of the initial condition, but with many fewer atoms near $p = 0$. Note that the values of K and $\bar{k}$ used here correspond to those used for the simulations in Fig. 2.

A scan with stochasticity parameter $K = 184$ at the quantum resonance $\bar{k} = 4\pi$ is shown in Fig. 5(d–f). The ballistic peaks are larger than those in Fig. 5(a–c), but the distribution is otherwise quite

similar. The peaks also appear to be moving more quickly than in any other cases shown, and appear to have left the visible region by the seventh kick.

Let us now compare our measured distributions with the results of numerical simulations that account for both the extended nature of our initial conditions and nonzero pulse durations. Fig. 6 shows the results of quantum simulations for the same parameters as the data shown in Fig. 5. The data and simulations shown in these two figures are plotted with both linear and logarithmic scales to facilitate comparison. The first case, shown in Fig. 6(a–c), corresponds to $\bar{k} = 2\pi$, $K = 82$, and was calculated with a 600 ns pulse width. The surface plot shows the curvature of the ballistic-peak trajectory, which closely follows the trajectory seen in Fig. 5(a–c).

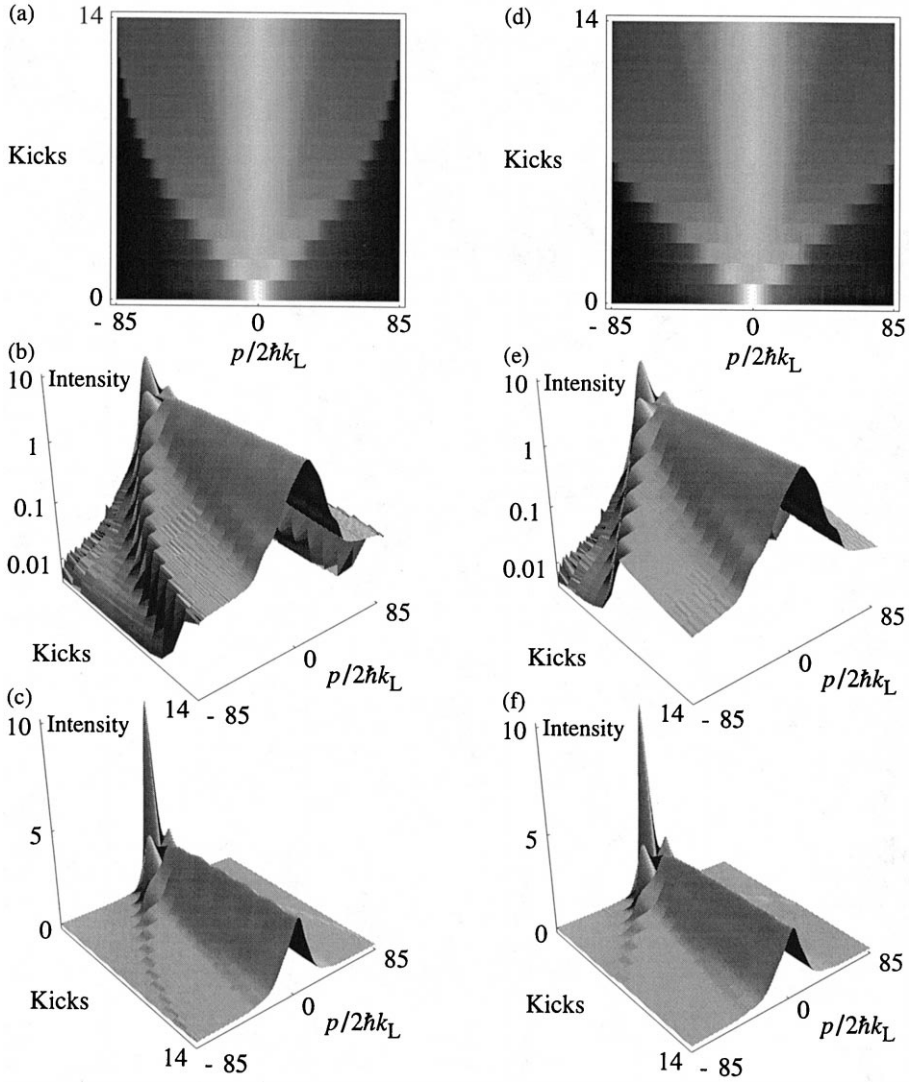

Fig. 6. Quantum simulations of momentum distribution evolution, for the same cases as the data shown in Fig. 5. The two cases are (a–c) near $\bar{k} = 2\pi$, with $K = 82$ and 600 ns pulses and (d–f) near $\bar{k} = 4\pi$, with $K = 184$ and 295 ns square pulses. The initial condition for both cases was a Gaussian with width $\sigma_p/2\hbar k_L = 4$. The evolution of the ballistic peaks closely matches that of the experimental data in Fig. 5. The remainder of the distribution undergoes motion that is primarily not resolved in the experiment.

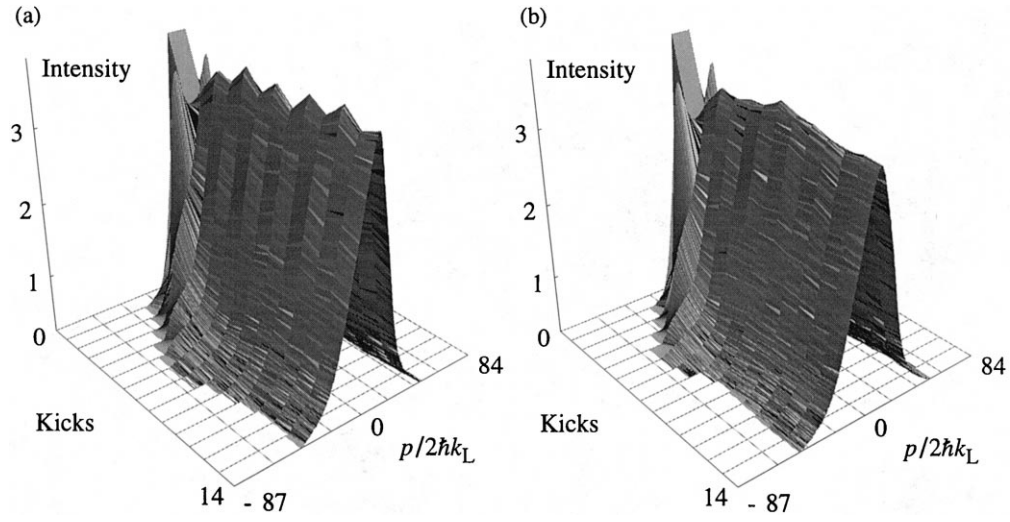

Fig. 7. Detail of the data shown in Fig. 5. Case (a), which is at $\bar{k} = 2\pi$ shows a small period-2 oscillation in intensity at $p = 0$ that follows the prediction for a quantum antiresonance (see Fig. 2). For case (b), near the full quantum resonance at $\bar{k} = 4\pi$, the period-2 oscillations are not observed. Note that similar behavior is visible at the appropriate scale in the simulations shown in Fig. 6. For both plots, the intensity scale is linear and the entire range is not shown.

The density plot of the same simulation shows a bright central region that does not undergo ballistic motion. Note that Fig. 2b shows a simulation with these parameters that uses δ-function pulses. A comparison of Fig. 2b and Fig. 6(a–c) shows the effects of nonzero-width pulses. The second case, shown in Fig. 6(d–f), represents $\bar{k} = 4\pi$ at $K = 184$, and was calculated with a 295 ns pulse width. The momentum boundary effects are present but not as strong in this case, as the ballistic peak trajectory is nearly straight. The peaks leave our detection region after about seven kicks, as we saw in the experiment (Fig. 5(d–f)).

Now that we have examined the behavior of the ballistic peaks, let us again consider the differences between the behavior at $\bar{k} = 2\pi$ and $\bar{k} = 4\pi$. Fig. 7 shows a magnified section of the data presented in Fig. 5, plotted with a linear intensity scale. It is possible to resolve features on this scale that were not visible in Fig. 5. The most striking feature of Fig. 7a is the period-2 oscillation present in the intensity at $p = 0$. These oscillations are a feature of the dynamics at $\bar{k} = 2\pi$ where the quantum phase factor between kicks alternates sign, and were not visible in the data taken with a weaker kicking strength. Oscillations of similar magnitude are present in the simulations shown in Fig. 6(a–c). The period-2 oscillations are not present in Fig. 7b, which presents data taken at $\bar{k} = 4\pi$. Likewise, the simulations at $\bar{k} = 4\pi$ shown in Fig. 6(d–f) do not exhibit period-2 oscillations.

Finally, let us note that while the ballistic peaks can clearly be resolved by eye in our measured distributions, it is harder to classify them by looking at the energy evolution. In the current generation of experiments, only a small fraction of the atoms are states that undergo ballistic motion. Colder initial conditions should enable a more detailed study of these dynamics.

5. Summary

We have observed the motion of ballistic peaks at the quantum resonance ($\bar{k} = 4\pi$) and at the quantum antiresonance ($\bar{k} = 2\pi$) in the quantum kicked rotor system. Qualitative agreement has been established between measured momentum distributions and quantum simulations about the location and behavior of these peaks. Further, we have experimentally resolved differences between the behavior of the system at the resonance and antiresonance due to their different natures.

Acknowledgements

This work was supported by the Robert A. Welch Foundation and the National Science Foundation. D.A.S. acknowledges support from the Fannie and John Hertz Foundation. Computations were performed on Texas Advanced Computing Center supercomputers.

References

[1] Casati, G., Chirikov, B.V., Ford, J., and Izrailev, F.M., Stochastic Behaviour in Classical and Quantum Hamiltonian Systems, Lecture Notes in Physics vol. 93, G. Casati, J. Ford (Eds.), Springer, Berlin, 1979.
[2] B. Chirikov, F.M. Izrailev, D.L. Shepelyansky, Sov. Sci. Rev. C 2 (1981) 209.
[3] Fishman, S., Grempel, D.R., and Prange, R.E., Phys. Rev. Lett. 49 (1982) 509; Grempel, D.R., Prange, R.E., and Fishman, S., Phys. Rev. A 29 (1984) 1639.
[4] D.L. Shepelyansky, Physica D 8 (1983) 208.
[5] Shepelyansky, D.L., Phys. Rev. Lett. 56 (1986) 677; Physica D 28 (1987) 103.
[6] D. Cohen, Phys. Rev. A 44 (1991) 2292.
[7] Blümel, R., and Reinhardt, W.P., Chaos in Atomic Physics, Cambridge, 1997.
[8] Izrailev, F.M., and Shepelyanskii, D.L., Sov. Phys. Dokl. 24 (1979) 996; Theor. Math. Phys. 43 (1980) 553.
[9] J.E. Bayfield, P.M. Koch, Phys. Rev. Lett. 33 (1974) 258.
[10] E.J. Galvez, B.E. Sauer, L. Moorman, P.M. Koch, D. Richards, Phys. Rev. Lett. 61 (1988) 2011.
[11] J.E. Bayfield, G. Casati, I. Guarneri, D.W. Sokol, Phys. Rev. Lett. 63 (1989) 364.
[12] R. Blümel, R. Graham, L. Sirko, U. Smilansky, H. Walther, K. Yamada, Phys. Rev. Lett. 62 (1989) 341.
[13] M. Arndt, A. Buchleitner, R.N. Mantegna, H. Walther, Phys. Rev. Lett. 67 (1991) 2435.
[14] R. Graham, M. Schlautmann, P. Zoller, Phys. Rev. A 45 (1992) R19.
[15] F.L. Moore, J.C. Robinson, C. Bharucha, P.E. Williams, M.G. Raizen, Phys. Rev. Lett. 73 (1994) 2974.
[16] J.C. Robinson, C. Bharucha, F.L. Moore, R. Jahnke, G.A. Georgakis, Q. Niu, M.G. Raizen, B. Sundaram, Phys. Rev. Lett. 74 (1995) 3963.
[17] F.L. Moore, J.C. Robinson, C.F. Bharucha, B. Sundaram, M.G. Raizen, Phys. Rev. Lett. 75 (1995) 4598.
[18] J.C. Robinson, C.F. Bharucha, K.W. Madison, F.L. Moore, B. Sundaram, S.R. Wilkinson, M.G. Raizen, Phys. Rev. Lett. 76 (1996) 3304.
[19] G.P. Collins, Phys. Today 48 (1995) 18.
[20] P.J. Bardroff, I. Bialynicki-Birula, D.S. Krähmer, G. Kurizki, E. Mayr, P. Stifter, W.P. Schleich, Phys. Rev. Lett. 74 (1995) 3959.
[21] C.F. Bharucha, J.C. Robinson, F.L. Moore, B. Sundaram, Q. Niu, M.G. Raizen, Phys. Rev. E 60 (1999) 3881.
[22] B.G. Klappauf, W.H. Oskay, D.A. Steck, M.G. Raizen, Physica D 131 (1999) 78.
[23] Oberthaler, M.K., Godun, R.M., d'Arcy, M.B., Summy, G.S., and Burnett, K., Phys. Rev. Lett. 83 (1999) 4447.
[24] G. Casati, J. Ford, I. Guarneri, F. Vivaldi, Phys. Rev. A 36 (1987) 2495.
[25] Reichl, L.E., The Transition to Chaos in Conservative Classical Systems: Quantum Manifestations, Springer-Verlag, Berlin, 1992.
[26] P.J. Martin, P.L. Gould, B.G. Oldaker, A.H. Miklich, D.E. Pritchard, Phys. Rev. A 36 (1987) 2495.
[27] Klappauf, B.G., Oskay, W.H., Steck, D.A., and Raizen, M.G., Phys. Rev. Lett. 81 (1998) 1203; Erratum, Phys. Rev. Lett. 82 (1999) 241.
[28] B.G. Klappauf, W.H. Oskay, D.A. Steck, M.G. Raizen, Phys. Rev. Lett. 81 (1998) 4044.
[29] S. Chu, Science 253 (1991) 861.
[30] Cohen-Tannoudji, C., in: J. Dalibard, J.M. Raimond, J. Zinn-Justin (Eds.), Fundamental Systems in Quantum Optics, Les Houches, 1990, Elsevier, London, 1992.